🍃

High-Efficiency Plug-and-Play Source of Heralded Single Photons

Nicola Montaut,[*] Linda Sansoni, Evan Meyer-Scott, Raimund Ricken, Viktor Quiring,
Harald Herrmann, and Christine Silberhorn

Integrated Quantum Optics, Universität Paderborn, Warburger Strasse 100, 33098 Paderborn, Germany

Reliable generation of single photons is of key importance for fundamental physical experiments and to demonstrate quantum protocols. Waveguide-based photon-pair sources have shown great promise in this regard due to their large spectral tunability, high generation rates, and long temporal coherence of the photon wave packet. However, integrating such sources with fiber-optic networks often results in a strong degradation of performance. We answer this challenge by presenting an alignment-free source of photon pairs in the telecommunications band that maintains heralding efficiency $> 50\%$ even after fiber pigtailing, photon separation, and pump suppression. The source combines this outstanding performance in heralding efficiency with a compact, stable, and easy-to-use "plug-and-play" package: one simply connects a laser to the input and detectors to the output, and the source is ready to use. This high performance can be achieved even outside the lab without the need for alignment which makes the source extremely useful for any experiment or demonstration needing heralded single photons.

I. INTRODUCTION

Using photons as carriers of quantum information has shown great potential for secure information exchange and resource-efficient computation [1] thanks to their lack of decoherence and suitability for long-distance transmission, namely, in optical fibers. Despite past successes, the implementation of quantum-information protocols beyond proof-of-principle demonstrations requires the development of reliable, accessible technology that respects the distinct and often more demanding physical regime of quantum light: different design criteria, low light intensity levels, and sensitivity to noise and loss.

The different regime to classical photonics becomes particularly critical when designing sources of photonic quantum states. Spontaneous parametric downconversion (SPDC), which is widely adopted for generation of quantum light, can be understood only by considering the quantum nature of the electromagnetic field interacting with a nonlinear medium. SPDC is stimulated from fluctuations of an infinitely broadband vacuum field, meaning excitation of all possible nonlinear processes occurs at random times and frequencies. Thus, the spectral properties of the generated light must be tailored and spurious processes suppressed by careful design of the nonlinear crystal. Compared to bulk crystals, periodically poled nonlinear waveguides allow for flexible control over these properties by engineering of the interaction length and poling period [2–15]. Furthermore, noise that cannot be suppressed through design must be filtered, which is challenging to integrate while maintaining low photon loss. The strong pump light, many orders of magnitude more intense than the single photons, must also be removed.

Losses pose a particular challenge to quantum photonic devices. In classical systems, losses can be compensated by amplifiers. But since quantum states cannot be deterministically amplified due to the no-cloning theorem [16], minimizing losses of each component is key, in particular, since important applications like quantum-information processing [17] and tests of Bell's inequality [18] are fundamentally intolerant to loss. Thus, low-loss interfaces between sources and optical-fiber networks [9,10,19–21] are vital. For stability and ease of use, permanent fixation of fibers is highly beneficial over free-space coupled devices.

The main challenge in exploiting quantum photon sources is the development of easy-to-handle and reliable components that also exhibit low loss, low noise, and the desired quantum properties. High performance is often strongly degraded when quantum devices are packaged [22–24]; therefore, most photon sources to date still rely on the careful alignment of external bulk components, limiting usefulness outside the lab.

Here, we present a "plug-and-play" source of telecom-wavelength heralded single photons that incorporates both desirable quantum properties suitable for long-distance applications [25] and an alignment-free packaging that allows for the use of this device outside the lab. This is a quantum source requiring no user intervention that produces photons with high heralding efficiency. In characterizing our device, we provide insight into which processes can be examined classically to predict the quantum performance, which quantum features are inaccessible with classical measurements, and cases where the classical
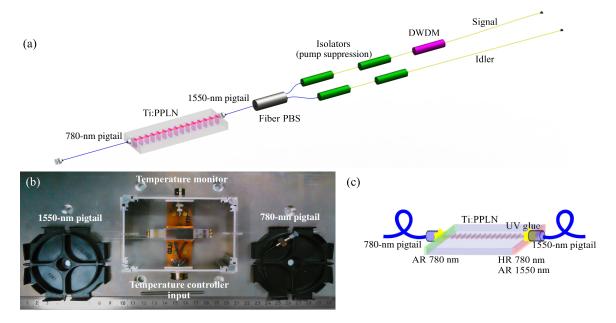
---

[*] montaut@mail.upb.de

FIG. 1.   (a) Schematic of the plug-and-play heralded single-photon source. (b) Image of the packaged waveguide chip. (c) Depiction of pigtailed chip. Abbreviations: Ti:PPLN, periodically poled titanium-indiffused lithium niobate; PBS, polarizing beam splitter; DWDM, dense-wavelength-division multiplexing filter; AR, antireflection; HR, high reflection.

characterization should have predictive power but often fails.

To remove the need of bulk components, we adopt a hybrid platform exploiting the high nonlinearity and low loss of periodically poled titanium-indiffused lithium niobate (Ti:PPLN) waveguides to produce photon pairs with high brightness, and standard telecommunications components for photon routing and filtering. The platforms are connected with a low-loss fiber pigtail. The lithium niobate and fiber-optic sections, thus, form a fully integrated source producing single photons in single-mode fiber already filtered and separated.

Previous fiber-pigtailed photon-pair sources [22,23] showed raw heralding efficiencies $\lesssim 3\%$, which we improve upon by more than 1 order of magnitude. By filtering only in one arm, we prevent losses in the transmitted photon and the resultant lowering of the heralding efficiency [26]. In addition, our source generates photons in the picosecond coherence range. This intermediate bandwidth regime shows promise in long-distance applications [25], as, like continuous-wave photons, they exhibit low dispersion when transmitted through fibers [27], and, like femtosecond photons, they can be engineered or filtered to produce spectrally pure states [28]. Overall, this device provides the necessary link to bridge the gap between experiments conducted in academic laboratories and real-world quantum applications.

II. DEVICE DESIGN

Our device takes advantage of high-efficiency parametric downconversion (PDC) based on the $\chi^{(2)}$ nonlinearity in

waveguides. Periodically poled titanium-indiffused waveguides in lithium niobate exhibit extremely low losses [29,30] and provide optical guiding in TE and TM polarizations, thereby allowing type-II PDC wherein an ordinarily polarized pump beam decays to orthogonally polarized photon pairs. This orthogonality provides easy separation of degenerate PDC photons based on their polarization, unlike type-0 sources [2,23,31,32] that split photons using 3-dB couplers which results in the loss of half of the generated photons. Additionally, type-II phase matching provides intrinsically narrow-band photons.

The fully fiber-pigtailed device is shown in Figs. 1(a) and 1(b). The Ti:PPLN waveguide chip can be temperature tuned via a built-in Peltier element. The waveguide is pigtailed with polarization-maintaining fibers (PMFs) on both end facets. The output fiber is spliced to a fiber polarizing beam splitter (fiber PBS), which separates the signal and idler into two spatial modes. Fiber isolators after the PBS ensure pump suppression, and a filter in the signal arm is used to remove noise and increase spectral purity.

III. DEVICE ENGINEERING

The waveguide and poling are designed to allow phase-matched PDC for a pump around 780 nm to degenerate photons around 1560 nm, and to optimize coupling to standard single-mode fibers. The fabrication proceeds as follows: 25-mm-long waveguides are produced by in-diffusing a titanium strip of 7 μm width and 80 nm thickness on a lithium niobate substrate at 1060 °C for 8.5 h. Next, the waveguides are periodically poled with period 9.08 μm for a length of 21 mm. The input facet of the chip
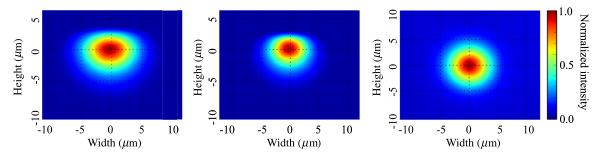
FIG. 2.   Measured optical field profiles of the TE (left), TM (center) modes in waveguide, and PANDA 1550-nm fiber mode (right).

receives an antireflective coating for the pump, and the output facet receives a high-reflective coating for the pump providing approximately 22-dB suppression and an anti-reflective coating for the photon pairs providing maximum coupling to the pigtailed fiber.

A crucial step of source preparation is to pigtail the front and rear ends by permanently fixing PMFs to the waveguide. To achieve the maximum coupling efficiency, we first measure the mode profiles of the waveguide (shown for both polarizations in Fig. 2) and standard 1550-nm PMFs. A broadband white light source at 1550 nm is used to couple light into the TE and TM polarization modes of the waveguide. Being broadband ($\Delta\lambda \approx 30$ nm), the source eliminates undesirable interference effects in the setup; however, it also introduces dispersion which blurs the measured modes. To minimize these effects, a 1-nm bandpass filter is added to the optical path. A 20× objective is used to inject light into a waveguide (or optical fiber). The modes are imaged using a 100× objective onto a Xenics infrared camera with a resolution of 20 μm/pixel. The full width at half maximum (FWHM) of the width and height of the TE (ordinary) mode of a 7-μm waveguide is measured to be 7.0 and 4.7 μm, respectively, and for the TM (extraordinary) mode, 5.3 and 3.4 μm, respectively. The asymmetry in the mode sizes is consistent with typical titanium-indiffused waveguides [33–35]. The measured mode diameter of a PMF mode is 6.08 μm. With these data, the mode profiles are modeled (FEMSIM package, RSOFT) to find maximum achievable coupling efficiencies between the waveguide and fiber modes for TE and TM of 92% and 85%, respectively.

The pigtailing of the output facet of the chip with a PMF is then carried out as follows: Broadband light at telecom wavelength is injected into the waveguide and collected using a PMF. The position of the fiber is controlled using a six-axis motorized stage that is capable of scanning in submicron resolutions along the end face of the waveguide. After performing multiple scan iterations of increasing resolution, the optimal position of the fiber is determined when maximum intensity of light coupled from the waveguide to the fiber for both TE and TM polarizations which is detected using a fiber PBS and photodiodes. Once the highest coupling is achieved, ultraviolet curing glue

(Norland Products Inc., NOA81) is applied at the interface between the PMF and chip and cured with an ultraviolet source [see Fig. 1(c)]. During the curing process, the position of the fiber shifts slightly thereby resulting in the lowering of the pigtailing efficiency of the TE mode from 88% (before curing) to $(83.8 \pm 1.8)\%$ and the TM mode from 80% to $(75.7 \pm 1.6)\%$. To pigtail the input side, we perform second-harmonic generation backwards in the sample, producing 780-nm light in the fundamental waveguide mode. We then optimize the coupling of this light to 780-nm PMF and glue as above. The coupling efficiency between the fiber and waveguide for pump wavelengths is measured to be $\eta_{\text{pump}} > 30\%$. The pigtailed chip is packaged and temperature controlled via a thermoelectric cooler which can operate at temperatures up to 70 °C. However, in this work all classical and quantum measurements are conducted at room temperature (25 °C) to produce degenerate single photons at telecom wavelength.

In order to separate the generated twin photons, we splice the output PMF to a fiber polarization beam splitter. A pair of C-band in-line isolators is then spliced to each arm of the fiber PBS to ensure pump suppression: each isolator provides 40- to 60-dB suppression for the pump due to the presence of a crystal that absorbs the pump. A fiber dense-wave-division multiplexing (DWDM) filter with a bandwidth of 200 GHz (1.6 nm) is also attached to the signal arm to remove noise and improve the purity of the heralded photons. To ensure maximum transmission, the idler arm remains unfiltered. The final device is completely alignment free and operates as a plug-and-play source of heralded single photons.

IV. RESULTS AND DISCUSSION

A. Classical characterization

An optimal source of quantum light should produce a large number of photon pairs (high brightness), which is related to the nonlinear conversion efficiency of the periodically poled waveguide. However, losses can drastically degrade the number of photons exiting from the device, despite the high internal brightness of the chip. For this reason, it is crucial to characterize both the nonlinear conversion efficiency and propagation losses. As classical
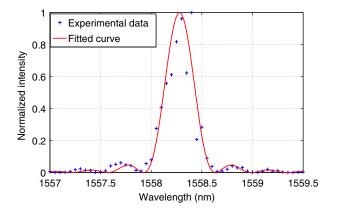
FIG. 3.   Second-harmonic generation intensity (blue markers) of the Ti:PPLN waveguide before pigtailing and the fitted sinc curve (red solid line) plotted versus SHG pump wavelength.

light is generally easier to generate and detect than quantum light, it is desirable to use classical characterization to predict quantum behavior. Hence, we look at the reverse process of PDC, that is, second-harmonic generation (SHG). This process is purely classical and thus provides only some information on the PDC emitted light, whose complete characterization requires quantum measurements. From SHG, we can estimate the phase-matching bandwidth, its central wavelength, and nonlinear conversion efficiency. We cannot, however, access the full spectrum of PDC photons or their spectral correlations, as these features emerge only from quantum measurements.

For SHG, a tunable continuous-wave laser at telecom wavelength is injected at 45° polarization into the waveguide chip (before pigtailing), and the generated light at twice the frequency is detected using a Si *p-i-n* diode. At room temperature (25 °C), the phase-matching peak, which corresponds to the degeneracy wavelength of the SHG process, is observed at 1558.29 nm, as shown in Fig. 3. The FWHM phase-matching bandwidth of (0.30 ± 0.02) nm is estimated from the SHG curve using the group refractive indices of LN. The measured SHG efficiency is determined using $\eta_{\mathrm{SHG}} = [P_{\mathrm{SHG}}/(P_{f,\mathrm{in}}^2 L^2)]100 = (2.36 \pm 0.21)\%$ W^{-1} cm^{-2}, where P_{SHG} is the output SHG power, $P_{f,\mathrm{in}}$ is the input power of the fundamental field, and L is the length of the poled region. For our type-II up-conversion process, the measured efficiency matches well with previous results [36], thereby showing that the device is capable of efficient photon-pair generation when operated in the quantum domain. We thus adopt this phase-matching condition for the production of degenerate heralded single photons.

The most important attribute of a heralded single-photon source is its ability to assure the presence of one photon by detecting the other (herald), known as the heralding efficiency. To predict the heralding efficiency, we estimate the transmission efficiency of the source by measuring the losses introduced by each component from the generation

point to the output. The waveguide losses are determined using the Fabry-Perot loss measurement technique [30] at 1550 nm. In TE polarization, the losses are measured to be (0.13 ± 0.02) dB/cm, and in TM, the losses are (0.18 ± 0.02) dB/cm. A fiber PBS is spliced to a pair of isolators on each arm, and the measured transmissions of the PBS-isolators combination are $(84.0 \pm 1.9)\%$ and $(81.5 \pm 1.9)\%$, respectively, for the TE and TM polarizations. The DWDM filter in the signal (TE-polarized) arm shows a transmission of $(86.0 \pm 2.0)\%$. The signal arm is used as the heralding arm, and hence the total transmission of this port does not affect the heralding efficiency of the idler photon. Therefore, the maximum heralding efficiency achievable in the idler (TM-polarized) arm is calculated to be $\eta_i^{\mathrm{calc}} = T_{\mathrm{WG,TM}} T_{\mathrm{FP,TM}} T_{\mathrm{PBS,TM}} = (58.6 \pm 3.3)\%$ before detection, where $T_{\mathrm{WG,TM}}$, $T_{\mathrm{FP,TM}}$, and $T_{\mathrm{PBS,TM}}$ are the transmission of the waveguide, fiber pigtail, and the PBS-isolator unit, respectively, for TM polarization. This classical estimation is an upper bound to the achievable heralding efficiency. In principle, the classical and quantum losses should be identical, but when dealing with PDC, background noise from the pump, fluorescence, or parasitic nonlinear processes can effectively lower the heralding efficiency [22,23,38,39] by increasing the heralding counts without a corresponding signal photon. We show in the following section that these effects are largely suppressed in our device, resulting in a heralding efficiency close to the classical value.

B. Quantum characterization

As the classical measurements provide limited information as discussed above, to fully characterize our source we must measure the photons produced by PDC directly. In the following section, we measure the brightness of the source, confirm the heralding efficiency matches the classical prediction, and investigate the spectral and modal properties of the quantum light.

An optimal source of heralded single photons should have high heralded photon rate and efficiency, emission of pure photon states, and, for long-distance communication, long coherence time. We show that these characteristics for our source reach or surpass the state of the art even after full fiber integration.

The setup used for the quantum measurements is shown in Fig. 4(a). A mode-locked Ti:sapphire laser that generates picosecond pulses with FWHM bandwidth 0.3 nm at 779.15-nm (phase-matched SHG wavelength) wavelength and 1-MHz repetition rate is used as the pump, with coupled powers of 1 to 30 μW. The photons are detected with superconducting nanowire single-photon detectors (SNSPDs, PhotonSpot) with detection efficiencies of $\eta_{\mathrm{det}} = (85 \pm 5)\%$.

As a first measurement, we look at the spectral brightness of our source, which is the rate at which the source generates photon pairs. The brightness of the
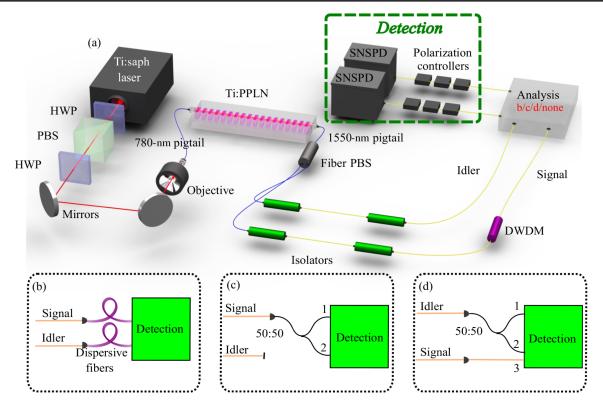
FIG. 4. (a) Schematic of the experimental setup used for efficiency measurements: The generated signal and idler photons pass directly to the detection unit or through one of the four quantum setups. (b) Joint spectral intensity measurement. (c) Unheralded $g^{(2)}(0)$ measurement. (d) Heralded $g^{(2)}(0)$ measurement. Abbreviations: HWP, half-wave plate; PBS, polarizing beam splitter; SNSPD, superconducting nanowire single-photon detector; 50:50, 50:50 coupler.

chip is measured to be $\mathcal{B}_{\text{chip}} = [(S_s S_i)/(C t P_{\text{chip}} \Delta \lambda_s)] = (1.39 \pm 0.04) \times 10^7 \frac{\text{pairs}}{\text{s mW nm}}$ at a mean photon number $\langle n \rangle \approx 0.01 \frac{\text{photons}}{\text{pulse}}$ (pump energy $E_{\text{pump}} = 3$ pJ/pulse), where t is the integration time, P_{chip} is the pump power coupled into the chip, and $\Delta \lambda_s$ is the bandwidth of the signal photon obtained from the joint spectral intensity (JSI) measurement. The source shows high generation rates, as expected from the nonlinear conversion efficiency measurement. It is higher than or similar to the brightness of other waveguide SPDC sources [12,15,21–23,40].

The heralding efficiency is determined using the apparatus as shown in Fig. 4(a) where the outputs of the device are directly connected to the SNSPDs. The raw heralding efficiency of the idler photon is given by $\eta_i = (C/S_s)$, where C are coincidences between the two outputs, S are singles counts, and s, i label the signal and idler, respectively. This is measured to be $\eta_i = (46.2 \pm 0.6)\%$. On correcting the raw value for the detector efficiency but retaining the channel losses (in contrast with Ref. [23]), we estimate the efficiency of the complete device from generation to output to be $\eta_i^{\text{corr}} = (\eta_i/\eta_{\text{det}}) = (54.4 \pm 3.3)\%$. This value is very close to the classically estimated maximum heralding efficiency that can be achieved from this device, a signature of minimized effects from spurious events. However, since the heralding efficiency is also

dependent on the noise counts in the optical channel, we characterize separately the background events. We measure that the singles count rates are approximately 9% background noise, which explains the slight difference in the measured and classically estimated heralding efficiency. In one year of operation since pigtailing, we find no degradation in the heralding efficiency or brightness of our source. In Table I, we compare our device with other benchmarked photon-pair sources that exploit either type-0, -I, or -II SPDC processes, with a focus on high heralding efficiency. Our results represent the best raw and detector-corrected heralding efficiencies when compared to other fiber-pigtailed sources [22,23] and closely approach the quality of state-of-the-art bulk sources. However, there is still room for improvement, particularly in the PBS and filters. Here, further integration will help, in particular, integrated PBSs [15] and/or wavelength division multiplexers [4,51] on chip for splitting of the photon pairs and pump suppression, respectively.

The spectral properties of PDC sources are related to the pump profile and phase-matching characteristics of the waveguide. Although SHG provides information on the spectral degeneracy and phase-matching bandwidth of the source, a thorough understanding of the spectral correlations can be obtained only by mapping the joint spectrum of the signal and idler photons. A time-of-flight

TABLE I. Comparison of different high-performance SPDC-based sources with respect to the type of source, central wavelength, photon bandwidth ($\Delta\lambda$), detector-corrected ($\eta_{s/i}^{corr}$), and raw ($\eta_{s/i}$) heralding efficiencies.

	Reference	Source	λ (nm)	$\Delta\lambda$ (nm)	$\eta_{s/i}^{corr}$ (%)	$\eta_{s/i}$ (%)
Free space	Kaneda *et al.* [41]	PPKTP/bulk	1590	1–4	87	7[a]
	Pomarico *et al.* [42]	PPLN/bulk	1550	3	80	8[a]
	Krapick *et al.* [43]	PPLN/WG	1575	$\cdots$	60	13.8[a]
	Bock *et al.* [14]	PPLN/WG	1312	$\cdots$	64.1	16[a]
	Guerreiro *et al.* [44]	KNbO$_3$/bulk	1550	$\cdots$	74.8[a]	18[a]
	Harder *et al.* [40]	PPKTP/WG	1536	5.1	80[a]	20.5
	Pereira *et al.* [45]	PPKTP/bulk	810	0.2	84	42.5[a]
	U'Ren *et al.* [46]	PPKTP/WG	800	2	85	51
	Weston *et al.* [47]	PPKTP/bulk	1570	15	80[a]	64
	Shalm *et al.* [48]	PPKTP/bulk	1550	$\cdots$	83.1[a]	75.6
	Giustina *et al.* [49]	PPKTP/bulk	810	$\cdots$	82.7[a]	78.6
	Ramelow *et al.* [11]	PPKTP/bulk	810	0.5	86.3[a]	82
Pigtailed	Zhong *et al.* [22]	PPKTP/WG	1316	1.3	13.7[a]	2.8
	Oesterling *et al.* [23]	PPLN/WG	1550	60	30.9[a]	3.1[a]
	Ngah *et al.* [50][b]	PPLN/WG	1540	0.25	42	7.1
	This work	PPLN/WG	1560	1.8	54.4	46.2

[a]is estimated from reported data.
[b]shows a source that is pigtailed only on the output side. Abbreviations: PPKTP, periodically poled potassium titanyl phosphate; PPLN, periodically poled lithium niobate; KNbO$_3$, potassium niobate; WG, waveguide.

spectrometer [52] as shown in Fig. 4(b) is used to measure the spectra of the PDC photons. The JSI and marginals of filtered and unfiltered PDC photons are shown in Fig. 5. The spectral bandwidth of the signal and idler photons are found to be $\Delta\lambda_s = (2.80 \pm 0.12)$ nm and $\Delta\lambda_i = (3.68 \pm 0.27)$ nm, respectively [see Figs. 5(a) and 5(c)]. Because of the tilt in our JSI, the signal photon has a narrower bandwidth and, hence, on applying the DWDM
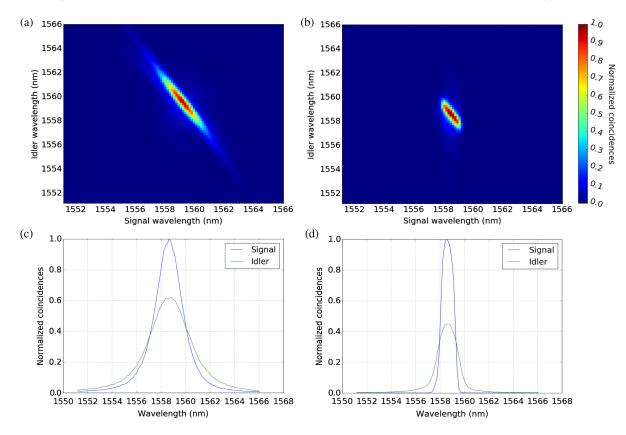

FIG. 5. Joint spectral intensities and marginals of (a),(c) unfiltered PDC and (b),(d) filter attached only on the signal arm. The marginals are the projection directly from the JSI and, thus, represent the heralded marginal spectra.

filter to this arm reduces the brightness less than if we applied it to the idler arm. The measured FWHM bandwidth is $\Delta\lambda_s = (1.06 \pm 0.02)$ nm and $\Delta\lambda_i = (1.83 \pm 0.04)$ nm for the signal and idler arms, respectively [see Figs. 5(b) and 5(d)] after filtering. The photon bandwidth of some other sources are listed in Table I. To estimate the temporal width of a coherent single-photon wave packet (here, referred to as the coherence time), we use the JSI to find the marginal spectrum of the idler when heralded by the signal at a single frequency. Taking the Fourier transform of this marginal spectrum provides the coherence time of the heralded photon of $\Delta\tau_{\rm sp} = (5.8 \pm 0.3)$ ps. From this, we find that the generated single photon can travel >130 km in a standard optical fiber before it starts to overlap with its neighboring pulses for a 1-GHz repetition rate. This is an order of magnitude higher than the equivalent possible distance for femtosecond photons ($\Delta\tau_{\rm sp} = 100$ fs), a gap maintained independent of repetition rates. This makes picosecond sources such as ours strongly desirable for long-distance quantum-communication applications.

Another important feature for a source such as ours is the spectral purity of the emitted single photons, which cannot be measured classically. Since in PDC photons are generated in pairs, any possible entanglement between them has the effect of reducing the purity of one photon when its twin is used as herald. To quantify the purity, we measure the degree of spectral entanglement present between the signal and idler photons. We directly characterize this property of our single-photon source by the unheralded second-order Glauber correlation function, $g^{(2)}(0)$. If the joint spectra are highly correlated, that is, consisting of multiple frequency modes, we expect a Poissonian photon number distribution corresponding to $g_P^{(2)}(0) = 1$. Alternatively, a decorrelated PDC spectrum corresponding to a spectrally pure state results in a thermal distribution with $g_{\rm th}^{(2)}(0) = 2$. Since the signal and idler share the same joint spectrum after filtering and heralding, the purity of the heralded idler photon (unfiltered) can be determined by measuring the purity of the signal photon (filtered). The setup required to measure the $g^{(2)}(0)$ is as shown in Fig. 4(c), where the signal photons are split by a 50:50 coupler then detected, giving $g_{s,{\rm raw}}^{(2)}(0) = 1.37 \pm 0.01$. Noise counts arising from fluorescence or other parasitic processes present in the signal strongly degrade the $g^{(2)}(0)$ value. The background events are measured by tuning the PDC spectrum away from the filter transmission band and recording only the triggered singles counts in both arms of the splitter. The background is estimated to be $(9.13 \pm 0.07)\%$ of the total singles counts. On correcting for these background counts [53], we get $g_s^{(2)}(0) = 1.66 \pm 0.05$ corresponding to a Schmidt number [54,55] $\mathcal{K} = 1.52$ and a purity $\mathcal{P} = 0.66 \pm 0.05$. We also estimate the spectral purity of our source from the joint spectra [56], which is determined to be $\mathcal{P} = 0.69$, which matches closely

with the unheralded $g^{(2)}(0)$ value. The purity can be improved by using filters with smaller bandwidth to minimize the correlations still present in the filtered spectrum; however, this comes at the cost of lowering the brightness and heralding efficiency of the source [26,57,58]. The nonclassicality of our source can also be demonstrated by analyzing the photon number correlations between signal and idler photons given by the second-order cross-correlation function [$g_{\rm cross}^{(2)}(0)$], which can be determined using the same measurement setup as the one used to measure heralding efficiency and brightness. The $g_{\rm cross}^{(2)}(0)$ of the source is measured to be $g_{\rm cross}^{(2)}(0) = [(CN_p)/(S_s S_i)] = 73.6 \pm 1.3$ at $\langle n \rangle \approx 0.01 \frac{\rm photons}{\rm pulse}$, where N_p is the number of pump trigger counts. This violates the Cauchy-Schwartz inequality [59] by more than 50 standard deviations, which confirms the quantum nature of our source in the photon number basis.

Finally, we have to ensure that our source produces single photons uncontaminated by multiphoton events and background light. This is done via a heralded $g^{(2)}(0)$ measurement, which also cannot be accomplished with classical techniques. An ideal single-photon source gives heralded $g_h^{(2)}(0) = 0$. In this case, the heralding photon is also detected, and the coincidences between all three detection events are analyzed [Fig. 4(d)]. The heralded second-order correlation is determined by $g_h^{(2)}(0) = [(C_{1,2,3}N_3)/(C_{1,3}C_{2,3})]$, where the number of two- and threefold coincidences are given by $C_{l,k}$ and $C_{l,k,m}$, respectively, where $l, k, m = \{1, 2, 3\}$ label the three outputs, and N_3 denotes the number of events in the heralding (signal) arm. We measure $g_{h,i}^{(2)}(0) = 0.014 \pm 0.001$ at $E_{\rm pump} = 2.4$ pJ/pulse, well below the threshold commonly used for single photons [$g_h^{(2)}(0) = 0.5$ [60]]. The measured value agrees well with the calculated value from multipair events [55,61] $g_{h,i}^{(2)}(0) \approx 0.013$ and is thus negligibly affected by other background light.

V. CONCLUSION

Following the increasing demand of stable, efficient, and reliable quantum devices for quantum-information applications, we experimentally demonstrate an efficient picosecond heralded single-photon source via type-II PDC in Ti:PPLN waveguides that is fully fiber integrated (including photon separation, pump suppression, and filtering), packaged, and ready to integrate with complex quantum systems. This device presents high stability and ease-of-use, together with quantum performances which exceed by far the packaged devices available up to now: low losses, high heralding efficiencies, and the ability to produce picosecond photons in the telecom regime. Owing to mature source engineering technology, the device offers complete flexibility to produce a large range of PDC

wavelengths and operation at nondegeneracy and can be integrated with a variety of filters for user-specific applications. In order to achieve a completely integrated device, the source can also be implemented by pumping with commercially available semiconductor lasers instead of a pulsed system as shown in this work. The quantum characteristics combined with the plug-and-play configuration of this source represent an advancement in the development of quantum-based technology for applications involving experimental verification of various communication protocols.

[1] I. L. Chuang and M. A. Nielsen, *Quantum Information and Quantum Computation* (Cambridge University Press, Cambridge, England, 2000).

[2] S. Tanzilli, H. De Riedmatten, H. Tittel, H. Zbinden, P. Baldi, M. De Micheli, D. B. Ostrowsky, and N. Gisin, Highly efficient photon-pair source using periodically poled lithium niobate waveguide, Electron. Lett. **37**, 26 (2001).

[3] G. Fujii, N. Namekata, M. Motoya, S. Kurimura, and S. Inoue, Bright narrowband source of photon pairs at optical telecommunication wavelengths using a type-II periodically poled lithium niobate waveguide, Opt. Express **15**, 12769 (2007).

[4] Q. Zhang, X. Xie, H. Takesue, S. W. Nam, C. Langrock, M. Fejer, and Y. Yamamoto, Correlated photon-pair generation in reverse-proton-exchange PPLN waveguides with integrated mode demultiplexer at 10 GHz clock, Opt. Express **15**, 10288 (2007).

[5] S. Zaske, A. Lenhard, and C. Becher, Efficient frequency downconversion at the single photon level from the red spectral range to the telecommunications *C*-band, Opt. Express **19**, 12825 (2011).

[6] T. Nosaka, B. Das, M. Fujimura, and T. Suhara, Cross-polarized twin photon generation device using quasi-phase matched LiNbO$_3$ waveguide, IEEE Photonics Technol. Lett. **18**, 124 (2006).

[7] J. Ghalbouni, I. Agha, R. Frey, E. Diamanti, and I. Zaquine, Experimental wavelength-division-multiplexed photon-pair distribution, Opt. Lett. **38**, 34 (2013).

[8] F. König, E. J. Mason, F. N. C. Wong, and M. A. Albota, Efficient and spectrally bright source of polarization-entangled photons, Phys. Rev. A **71**, 033805 (2005).

[9] Y.-K. Jiang and A. Tomita, The generation of polarization-entangled photon pairs using periodically poled lithium niobate waveguides in a fibre loop, J. Phys. B **40**, 437 (2007).

[10] S. Arahira, N. Namekata, T. Kishimoto, H. Yaegashi, and S. Inoue, Generation of polarization entangled photon pairs at telecommunication wavelength using cascaded $\chi^{(2)}$ processes in a periodically poled LiNbO$_3$ ridge waveguide, Opt. Express **19**, 16032 (2011).

[11] S. Ramelow, A. Mech, M. Giustina, S. Gröblacher, W. Wieczorek, J. Beyer, A. Lita, B. Calkins, T. Gerrits, S. W. Nam, A. Zeilinger, and R. Ursin, Highly efficient heralding of entangled single photons, Opt. Express **21**, 6707 (2013).

[12] H. Herrmann, X. Yang, A. Thomas, A. Poppe, W. Sohler, and C. Silberhorn, Post-selection free, integrated optical source of non-degenerate, polarization entangled photon pairs, Opt. Express **21**, 27981 (2013).

[13] I. Herbauts, B. Blauensteiner, A. Poppe, T. Jennewein, and H. Hübel, Demonstration of active routing of entanglement in a multi-user network, Opt. Express **21**, 29013 (2013).

[14] M. Bock, A. Lenhard, C. Chunnilall, and C. Becher, Highly efficient heralded single-photon source for telecom wavelengths based on a PPLN waveguide, Opt. Express **24**, 23992 (2016).

[15] L. Sansoni, K. H. Luo, C. Eigner, R. Ricken, V. Quiring, H. Herrmann, and C. Silberhorn, A two-channel, spectrally degenerate polarization entangled source on chip, npj Quantum Inf. **3**, 5 (2017).

[16] W. Wooters and W. Zurek, Quantum no-cloning theorem, Nature (London) **299**, 802 (1982).

[17] M. Varnava, D. E. Browne, and T. Rudolph, How Good Must Single Photon Sources and Detectors Be for Efficient Linear Optical Quantum Computation?, Phys. Rev. Lett. **100**, 060502 (2008).

[18] P. H. Eberhard, Background level and counter efficiencies required for a loophole-free Einstein-Podolsky-Rosen experiment, Phys. Rev. A **47**, R747 (1993).

[19] S. Arahira, T. Kishimoto, and H. Murai, 1.5-μm band polarization entangled photon-pair source with variable Bell states, Opt. Express **20**, 9862 (2012).

[20] T. Meany, L. A. Ngah, M. J. Collins, A. S. Clark, R. J. Williams, B. J. Eggleton, M. J. Steel, M. J. Withford, O. Alibart, and S. Tanzilli, Hybrid photonic circuit for multiplexed heralded single photons, Laser Photonics Rev. **8**, L42 (2014).

[21] F. Kaiser, B. Fedrici, A. Zavatta, V. D'Auria, and S. Tanzilli, A fully guided-wave squeezing experiment for fiber quantum networks, Optica **3**, 362 (2016).

[22] T. Zhong, F. N. C. Wong, T. D. Roberts, and P. Battle, High performance photon-pair source based on a fiber-coupled periodically poled KTiOPO$_4$ waveguide, Opt. Express **17**, 12019 (2009).

[23] L. Oesterling, F. Monteiro, S. Krupa, D. Nippa, R. Wolterman, D. Hayford, E. Stinaff, B. Sanguinetti, H. Zbinden, and R. Thew, Development of photon pair sources using periodically poled lithium niobate waveguide technology and fiber optic components, J. Mod. Opt. **62**, 1722 (2015).

[24] A. Schlehahn, S. Fischbach, R. Schmidt, A. Kaganskiy, A. Strittmatter, S. Rodt, T. Heindel, and S. Reitzenstein, A stand-alone fiber-coupled single-photon source, arXiv: 1703.10536.

[25] K. Sedziak, M. Lasota, and P. Kolenderski, Reducing detection noise of a photon pair in a dispersive medium by controlling its spectral entanglement, Optica 4, 84 (2017).

[26] E. Meyer-Scott, N. Montaut, J. Tiedau, L. Sansoni, H. Herrmann, T. J. Bartley, and C. Silberhorn, Limits on the heralding efficiencies and spectral purities of spectrally filtered single photons from photon-pair sources, Phys. Rev. A 95, 061803 (2017).

[27] T. Inagaki, N. Matsuda, O. Tadanaga, M. Asobe, and H. Takesue, Entanglement distribution over 300 km of fiber, Opt. Express 21, 23241 (2013).

[28] W. P. Grice and I. A. Walmsley, Spectral information and distinguishability in type-II down-conversion with a broadband pump, Phys. Rev. A 56, 1627 (1997).

[29] R. Schmidt and I. Kaminow, Metal-diffused optical waveguides in LiNbO$_3$, Appl. Phys. Lett. 25, 458 (1974).

[30] R. Regener and W. Sohler, Loss in low-finesse Ti:LiNbO$_3$ optical waveguide resonators, Appl. Phys. B 36, 143 (1985).

[31] S. Tanzilli, W. Tittel, H. De Riedmatten, H. Zbinden, P. Baldi, M. DeMicheli, D. Ostrowsky, and N. Gisin, PPLN waveguide for quantum communication, Eur. Phys. J. D 18, 155 (2002).

[32] H. Hubel, D. R. Hamel, A. Fedrizzi, S. Ramelow, K. J. Resch, and T. Jennewein, Direct generation of photon triplets using cascaded photon-pair sources, Nature (London) 466, 601 (2010).

[33] J. White and P. Heidrich, Optical waveguide refractive index profiles determined from measurement of mode indices: A simple analysis, Appl. Opt. 15, 151 (1976).

[34] M. Minakata, S. Saito, M. Shibata, and S. Miyazawa, Precise determination of refractive-index changes in Ti-diffused LiNbO$_3$ optical waveguides, J. Appl. Phys. 49, 4677 (1978).

[35] K. Sugii, M. Fukuma, and H. Iwasaki, A study on titanium diffusion into LiNbO$_3$ waveguides by electron probe analysis and x-ray diffraction methods, J. Mater. Sci. 13, 523 (1978).

[36] Type-II SHG efficiency is dependent on the d_{31} nonlinear coefficient, which is nearly 7 times smaller than the d_{33} exploited in a type-0 process. This results in a lowering of the type-II SHG efficiency by about 50 times compared to the type-0 process. Thus, our results are just slightly below one of the highest type-0 SHG efficiencies reported so far in LN, 150 % W^{-1} cm^{-2} [37].

[37] K. R. Parameswaran, R. K. Route, J. R. Kurz, R. V. Roussev, M. M. Fejer, and M. Fujimura, Highly efficient second-harmonic generation in buried waveguides formed by annealed and reverse proton exchange in periodically poled lithium niobate, Opt. Lett. 27, 179 (2002).

[38] J. S. Neergaard-Nielsen, B. M. Nielsen, H. Takahashi, A. I. Vistnes, and E. S. Polzik, High purity bright single photon source, Opt. Express 15, 7940 (2007).

[39] P. B. Dixon, D. Rosenberg, V. Stelmakh, M. E. Grein, R. S. Bennink, E. A. Dauler, A. J. Kerman, R. J. Molnar, and F. N. C. Wong, Heralding efficiency and correlated-mode coupling of near-IR fiber-coupled photon pairs, Phys. Rev. A 90, 043804 (2014).

[40] G. Harder, V. Ansari, B. Brecht, T. Dirmeier, C. Marquardt, and C. Silberhorn, An optimized photon pair source for quantum circuits, Opt. Express 21, 13975 (2013).

[41] F. Kaneda, K. Garay-Palmett, A. B. U'Ren, and P. G. Kwiat, Heralded single-photon source utilizing highly non-degenerate, spectrally factorable spontaneous parametric downconversion, Opt. Express 24, 10733 (2016).

[42] E. Pomarico, B. Sanguinetti, T. Guerreiro, R. Thew, and H. Zbinden, MHz rate and efficient synchronous heralding of single photons at telecom wavelengths, Opt. Express 20, 23846 (2012).

[43] S. Krapick, H. Herrmann, V. Quiring, B. Brecht, H. Suche, and C. Silberhorn, An efficient integrated two-color source for heralded single photons, New J. Phys. 15, 033010 (2013).

[44] T. Guerreiro, A. Martin, B. Sanguinetti, N. Bruno, H. Zbinden, and R. Thew, High efficiency coupling of photon pairs in practice, Opt. Express 21, 27641 (2013).

[45] M. D. C. Pereira, F. E. Becerra, B. L. Glebov, J. Fan, S. W. Nam, and A. Migdall, Demonstrating highly symmetric single-mode, single-photon heralding efficiency in spontaneous parametric downconversion, Opt. Lett. 38, 1609 (2013).

[46] A. B. U'Ren, C. Silberhorn, K. Banaszek, and I. A. Walmsley, Efficient Conditional Preparation of High-Fidelity Single Photon States for Fiber-Optic Quantum Networks, Phys. Rev. Lett. 93, 093601 (2004).

[47] M. M. Weston, H. M. Chrzanowski, S. Wollmann, A. Boston, J. Ho, L. K. Shalm, V. B. Verma, M. S. Allman, S. W. Nam, R. B. Patel et al., Efficient and pure femtosecond-pulse-length source of polarization-entangled photons, Opt. Express 24, 10869 (2016).

[48] L. K. Shalm et al., Strong Loophole-Free Test of Local Realism, Phys. Rev. Lett. 115, 250402 (2015).

[49] M. Giustina et al., Significant-Loophole-Free Test of Bell's Theorem with Entangled Photons, Phys. Rev. Lett. 115, 250401 (2015).

[50] L. A. Ngah, O. Alibart, L. Labonté, V. D'Auria, and S. Tanzilli, Ultra-fast heralded single photon source based on telecom technology, Laser Photonics Rev. 9, L1 (2015).

[51] H. Jin, F. M. Liu, P. Xu, J. L. Xia, M. L. Zhong, Y. Yuan, J. W. Zhou, Y. X. Gong, W. Wang, and S. N. Zhu, On-Chip Generation and Manipulation of Entangled Photons Based on Reconfigurable Lithium-Niobate Waveguide Circuits, Phys. Rev. Lett. 113, 103601 (2014).

[52] M. Avenhaus, A. Eckstein, P. J. Mosley, and C. Silberhorn, Fiber-assisted single-photon spectrograph, Opt. Lett. 34, 2873 (2009).

[53] A. Eckstein, A. Christ, P. J. Mosley, and C. Silberhorn, Realistic $g^{(2)}$ measurement of a PDC source with single photon detectors in the presence of background, Phys. Status Solidi C 8, 1216 (2011).

[54] A. Eckstein, A. Christ, P. J. Mosley, and C. Silberhorn, Highly Efficient Single-Pass Source of Pulsed Single-Mode Twin Beams of Light, Phys. Rev. Lett. 106, 013603 (2011).

[55] A. Christ, K. Laiho, A. Eckstein, K. N. Cassemiro, and C. Silberhorn, Probing multimode squeezing with correlation functions, New J. Phys. 13, 033027 (2011).

[56] K. N. Cassemiro, K. Laiho, and C. Silberhorn, Accessing the purity of a single photon by the width of the Hong-Ou-Mandel interference, New J. Phys. **12**, 113052 (2010).

[57] T. Aichele, A. I. Lvovsky, and S. Schiller, Optical mode characterization of single photons prepared by means of conditional measurements on a biphoton state, Eur. Phys. J. D **18**, 237 (2002).

[58] P. Aboussouan, O. Alibart, D. B. Ostrowsky, P. Baldi, and S. Tanzilli, High-visibility two-photon interference at a telecom wavelength using picosecond-regime separated sources, Phys. Rev. A **81**, 021801 (2010).

[59] R. Loudon, *The Quantum Theory of Light* (Oxford University Press, Oxford, 2000).

[60] M. Leifgen, T. Schröder, F. Gädeke, R. Riemann, V. Métillon, E. Neu, C. Hepp, C. Arend, C. Becher, K. Lauritsen, and O. Benson, Evaluation of nitrogen- and silicon-vacancy defect centres as single photon sources in quantum key distribution, New J. Phys. **16**, 023021 (2014).

[61] K. Laiho, A. Christ, K. Cassemiro, and C. Silberhorn, Testing spectral filters as Gaussian quantum optical channels, Opt. Lett. **36**, 1476 (2011).

[62] http://www.picque.eu.